Physics of Fluids

Pressure-sensitive ion conduction in a conical channel: Optimal pressure and geometry

Cite as: Phys. Fluids **34**, 101701 (2022); https://doi.org/10.1063/5.0113035
Submitted: 22 July 2022 • Accepted: 01 September 2022 • Published Online: 03 October 2022

Willem Q. Boon, Tim E. Veenstra, Marjolein Dijkstra, et al.

Physics of Fluids LETTER scitation.org/journal/phf

Pressure-sensitive ion conduction in a conical channel: Optimal pressure and geometry

Cite as: Phys. Fluids **34**, 101701 (2022); doi: 10.1063/5.0113035
Submitted: 22 July 2022 · Accepted: 1 September 2022 ·
Published Online: 3 October 2022

Willem Q. Boon,[1] Tim E. Veenstra,[1] Marjolein Dijkstra,[2] and René van Roij[1,a)]

AFFILIATIONS

[1]Institute for Theoretical Physics, Utrecht University, Princetonplein 5, 3584 CC Utrecht, The Netherlands
[2]Soft Condensed Matter, Debye Institute for Nanomaterials Science, Utrecht University, Princetonplein 1, 3584 CC Utrecht, The Netherlands

[a)]Author to whom correspondence should be addressed: r.vanroij@uu.nl

ABSTRACT

Using both analytic and numerical analyses of the Poisson–Nernst–Planck equations, we theoretically investigate the electric conductivity of a conical channel which, in accordance with recent experiments, exhibits a strong non-linear pressure dependence. This mechanosensitive diodic behavior stems from the pressure-sensitive build-up or depletion of salt in the pore. From our analytic results, we find that the optimal geometry for this diodic behavior strongly depends on the flow rate with the ideal ratio of tip-to-base-radii being equal to 0.22 at zero-flow. With increased flow, this optimal ratio becomes smaller and, simultaneously, the diodic performance becomes weaker. Consequently an optimal diode is obtained at zero-flow, which is realized by applying a pressure drop that is proportional to the applied potential and to the inverse square of the tip radius, thereby countering electro-osmotic flow. When the applied pressure deviates from this ideal pressure drop the diodic performance falls sharply, explaining the dramatic mechanosensitivity observed in experiments.

A fluidic channel allows for the simultaneous transport of solvent, charge, and dissolved salt when connected to two liquid electrolyte reservoirs at different pressures, voltages, salt concentrations, and/or temperatures. Such ionic transport is not only interesting from a fundamental point of view but also for energy harvesting,[1–4] desalination,[5,6] and microfluidic applications.[7,8] In all these devices fluidic channels with dimensions in the nano- and micrometer regime are used,[9–11] a size range where the influence of surface charge on transport becomes significant due to the relatively large surface-to-volume ratio. This surface charge is key to electrokinetic transduction phenomena, such as the flow of electrolyte by an electric potential drop (electro-osmosis) or the electric (streaming) current induced by flow due to an applied pressure drop.[12–14] While these electrokinetic transduction phenomena have long been understood,[15–18] at least in simple channel geometries, in conical pores, exotic transport behaviors, such as electro-osmotic flow inversion,[19–21] other non-linear flow-effects,[22,23] and current rectification,[24–30] have been observed. Such non-linear transport behavior makes conical pores uniquely attractive for biochemical sensing[31–38] and neuromorphic applications.[39–42] In this Letter, we analyze the intricate case of a micrometer-sized cone-shaped channel exposed to a simultaneous pressure and electric potential drop by means of the well-known Poisson–Nernst–Planck–Stokes (PNPS) equations. We will show that the ionic current in conical nanopores can be either strongly reduced or enhanced by a pressure difference and concomitant flow, resulting in an extremely mechanosensitive ionic diode similar to those present in cell membranes.[43,44] Such pressure-sensitivity can also be used to optimize power generation in artificial pores.[45] Recent experiments revealed such a non-linear pressure-induced electric transport in conical pores even at micrometer length scales.[46] It was found that the electric current $I(\Delta P, \Delta\psi)$, due to an applied potential difference $\Delta\psi$, is very sensitively dependent on the applied pressure drop ΔP over the channel. Surprisingly, the observed pressure dependence of the electric conductance occurred at extremely low rather than high pressures. For conical pores it was already observed that, for $\Delta P = 0$, the response of the current I is asymmetric with regard to the sign of $\Delta\psi$ and this so-called current rectification is attributed to concentration polarization.[24–30,47] Here, we show that the flow (and hence pressure)-sensitive conductivity for $\Delta P \neq 0$ can also be understood by the concentration-polarization, in contrast to earlier work which suggests that novel mechanisms are needed, such as a bulk space-charge[46] or a non-linear streaming current.[45] Such a flow-sensitive conduction was previously noted in numerical calculations, which, however, ignored electro-osmotic flow[48] that we find to be of great importance. Whether

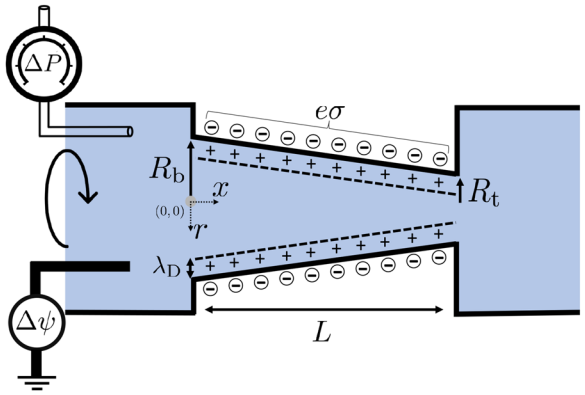

FIG. 1. Schematic of an axially symmetric conical channel of length L, base radius R_b at $x=0$, and tip radius $R_t \leq R_b$ at $x=L$. The channel connects two bulk 1:1 electrolytes in the half spaces $x<0$ and $x>L$. The channel wall carries a negative surface charge density $e\sigma$ that induces an electric double layer of thickness λ_D, the Debye length. Volume, charge, and salt ions are transported through the channel by an applied potential drop $\Delta\psi$ and pressure drop ΔP.

electro-osmotic flow can[24,50–52] or cannot[53–56] be ignored is debated in the literature and we reconcile these two opposing views by showing that the importance of flow depends on Péclet number; in the small Péclet regime[24] the flow can be ignored while in the large Péclet regime[53] it is important. This large-Pe regime is natural for large micrometer channels[29,30,46,57,58] common in experiments, while theoretical descriptions of such systems often neglect flow.[51,60,61] To account for the effect of flow on rectification, we derive for the first time a closed-form expression for the ion-distribution in the channel. Together with the 2×2 transport matrix accounting for both the pressure-driven flow and the electro-osmotic flow neglected by Ref. 48, this concentration profile naturally accounts for the mechanosensitive cone conductance, without needing to invoke any novel coupling between current and the Maxwell stress-tensor as was done in Ref. 46. Such a pressure-sensitivity cannot be captured by recent analytic theories as they neglect flow entirely.[59,60] Furthermore, we find that the optimal cone geometry for rectification strongly depends on the flow rate, while studies searching numerically for such a geometry often neglect exactly this feature.[49,52,62]

As depicted in Fig. 1 we consider two reservoirs of an aqueous 1:1 electrolyte in the two half spaces $x<0$ and $x>L$ connected by an axially symmetric cone-shaped channel of length L. Here, x is the Cartesian coordinate along the symmetry axis; the radial coordinate is r. The channel has a wide base radius $R_b \ll L$ at $x=0$ and a narrow tip radius $R_t \leq R_b$ at $x=L$. The radius of the channel for $x\in[0,L]$ reads $R(x)=R_b-(x/L)(R_b-R_t)$. The channel wall at $r=R(x)$ carries a uniform negative surface charge density $e\sigma$, with e being the proton charge. The two reservoirs both contain an identical aqueous 1:1 electrolyte with viscosity η, ionic diffusion coefficient D, dielectric permittivity ε, and total ionic bulk concentration $2\rho_b$. Thus, asymptotically far from the channel, at either side $|x|/L\gg1$, the local cation concentration $\rho_+(x,r)$ and anion concentration $\rho_-(x,r)$ are both equal to ρ_b.

Inspired by the experiments of Ref. 46, we consider an applied pressure drop ΔP and a simultaneous electric potential drop $\Delta\psi$ across the channel. These steady driving forces give rise to a potential $\psi(x,r)$ and a pressure excess $P(x,r)-P_0$ which vanish in the bulk phase $x\gg L$ and are equal to $\Delta\psi$ and ΔP, respectively, for $x\ll -L$, where P_0 is an arbitrary reference pressure. They drive a fluid flow with velocity $\mathbf{u}(x,r)$ and ionic fluxes $\mathbf{j}_\pm(x,r)$, leading to nontrivial concentration profiles $\rho_\pm(x,r)$. In part (I) of the supplementary material, we present the standard Poisson–Nernst–Planck–Stokes (PNPS) equations and the blocking and no-slip boundary conditions. Together with Gauss' law for the surface charge, they form a closed set for $\mathbf{u}$, ψ, $\mathbf{j}_\pm$, and $\rho_\pm$. Convenient linear combinations are the total salt concentration $\rho_s=\rho_++\rho_-$, the charge density $\rho_e=\rho_+-\rho_-$, and the associated fluxes $\mathbf{j}_s=\mathbf{j}_++\mathbf{j}_-$ and $\mathbf{j}_e=\mathbf{j}_+-\mathbf{j}_-$. In equilibrium, i.e., for vanishing ΔP and $\Delta\psi$, all fluxes vanish and the PNPS equations describe an Electric Double Layer (EDL) with an excess of cations and a depletion of anions close to $r=R(x)$ such that the negative surface charge is compensated.[62] The thickness of the EDL is given by the Debye length $\lambda_D=\sqrt{\varepsilon k_BT/2e^2\rho_b}=10$ nm for the case $\rho_b=1$ mM that we consider.

Inspired by the experimental conditions of Ref. 46, the focus of this Letter will be on the long-channel thin-EDL limit with $L\gg R_b\geq R_t\gg\lambda_D$ such that EDL-overlap does not play a role. This is in contrast to a large body of literature on non-linear transport in cone-shaped channels, where overlap of the EDL is a key ingredient for current rectification and diodic behavior.[24–26] We will show that the conical geometry combined with simultaneous pressure- and potential-induced transport leads to an x-independent volumetric flow rate $Q=2\pi\hat{\mathbf{x}}\cdot\int_0^{R(x)}\mathbf{u}(x,r)rdr$ and electric current $I=2\pi e\hat{\mathbf{x}}\cdot\int_0^{R(x)}\mathbf{j}_e(x,r)rdr$ that satisfy an Onsager-like relation

$$\begin{pmatrix}Q\\ I\end{pmatrix}=\frac{\pi R_bR_t}{L}\begin{pmatrix}\mathbb{L}_{11} & \mathbb{L}_{12}\\ \mathbb{L}_{21} & \mathbb{L}_{22}(\Delta P,\Delta\psi)\end{pmatrix}\begin{pmatrix}\Delta P\\ \Delta\psi\end{pmatrix}. \tag{1}$$

We set out to calculate all elements of the transport matrix $\mathbb{L}$ analytically, not only the permeability $\mathbb{L}_{11}$ and the electro-osmotic mobility $\mathbb{L}_{12}=\mathbb{L}_{21}$ but also the electric conductance $\mathbb{L}_{22}$ that, as we will see, strongly depends on the applied pressure and voltage drop in agreement with experiments.[46] This pressure-sensitivity is due to highly nontrivial ion concentration profiles that vary on length scales of the channel dimensions as follows from our analytic expression obtained from the PNPS equations. From this, we will find that optimal current rectification requires not only a pressure drop $\Delta P^*=-\mathbb{L}_{12}\Delta\psi/\mathbb{L}_{11}$ (such that $Q=0$) but also a universal optimal geometry with $R_t/R_b\simeq0.22$. We solve the PNPS equations for a wide variety of system parameters and show illustrative examples for the standard parameter set inspired by Ref. 46 with tip radius $R_t=0.17\mu$m, channel length $L=10\mu$ m, base radius $R_b=1.04\mu$ m, viscosity $\eta=1$ mPa s, dielectric constant 80 times vacuum permittivity, ionic diffusion coefficient $D=1\,\mathrm{nm}^2/\mathrm{ns}$, and surface charge $e\sigma=-0.02e/\mathrm{nm}^2$, which gives at $\rho_b=1$ mM a zeta potential of $\psi_0=-40$ mV corresponding to a silica surface in contact with an aqueous 1:1 electrolyte.[63] In line with the Stokes equation, we find $\mathbf{u}(x,r)$ to contain essentially two contributions. (i) A pressure drop on its own induces a Poiseuille-like flow that is directed toward the (virtual) vertex of the cone for $\Delta P>0$ or away from it for $\Delta P<0$.[64–66] Its contribution $Q_P\equiv(\pi R_bR_t/L)\mathbb{L}_{11}\Delta P$ to Q is independent of x and can be obtained analytically[64–66] to yield $\mathbb{L}_{11}=R_b^2R_t^2/8\eta\langle R^2\rangle$, where the angular brackets denote a lateral average $\langle R^2\rangle=\int_0^L R^2(x)\mathrm{d}x/L=(R_b^2+R_t^2+R_bR_t)/3$. The excellent agreement between the pressure-drop dependence of our linear expression for Q_P and our

numerically obtained value of Q at $\Delta\psi = 0$ is shown in Fig. S1(a) of part (II) in the supplementary material. (ii) For our negative surface charge, the potential drop $\Delta\psi$ on its own induces an electro-osmotic plug-like flow toward the tip of the cone for $\Delta\psi > 0$ or away from the tip for $\Delta\psi < 0$. We are not aware of an explicit expression in the literature for $\mathbb{L}_{12}$ that characterizes the electro-osmotic flow rate $Q_\psi \equiv (\pi R_b R_t/L)\mathbb{L}_{12}\Delta\psi$ in a conical pore. Here, we derive an explicit expression for $\mathbb{L}_{12}$, which first requires an expression for the cross-sectional averaged electric field $-\partial_x\bar{\psi}(x)$, see Eq. (S1) of part (II) in the supplementary material, where $\bar{\psi}(x) = 2\pi\int_0^{R(x)}\psi(x,r)r\mathrm{d}r/\ \pi R^2(x)$. This averaged electric field has to be proportional to the inverse of the cross section $\pi R^2(x)$ in order to be divergence free. The proportionality constant follows, in the long-channel limit, from the condition that $\int_0^L \partial_x\bar{\psi}(x)\mathrm{d}x = -\Delta\psi$. This yields

$$\partial_x\bar{\psi}(x) = -\frac{\Delta\psi}{L}\frac{R_b R_t}{R^2(x)}, \tag{2}$$

which compares well to the numerical results, as illustrated in Fig. S2 of part (II) in the supplementary material. Using the standard electro-osmotic mobility $\mathbb{L}_{12} = -\varepsilon\psi_0/\eta$ for a cylinder,[67] but now with our laterally varying electric field and radius, we obtain $Q_\psi = \pi R^2(x)(-\varepsilon\psi_0/\eta)\partial_x\bar{\psi}(x)$ which with Eq. (2) is independent of x and hence represents a valid divergence-free solution for the stationary state. In Fig. S1(b) of part (II) in the supplementary material, we compare this expression for Q_ψ as a function of $\Delta\psi$ with numerical calculations. The agreement is good, although minor deviations on the order of $\sim$10% are visible which we attribute to the approximate nature of our $\mathbb{L}_{12}$.

With $\mathbb{L}_{11}$ and $\mathbb{L}_{12}$ established, we continue with $\mathbb{L}_{22}$, for which the total ion concentration $\rho_s(x,r)$ is expected to play a major role. In our numerical calculations, we find weak radial variation of $\rho_s(x,r)$ outside the EDL-vicinity $r \simeq R(x)$, in agreement with Ref. 48. Hence, within the thin-EDL limit, this implies that the cross-sectional averaged concentration $\bar{\rho}_s(x)$ is a good proxy for the salt concentration at axial position x. If we now define the total salt flux as $J(x) = 2\pi\hat{\mathbf{x}}\cdot\int_0^{R(x)}\mathbf{j}_s(x,r)r\mathrm{d}r$, we can insert the diffusive, conductive, and advective contributions of $\mathbf{j}_s$ as given by the PNPS equations in part (I) of the supplementary material to rewrite the stationarity condition $\partial_x J(x) = 0$ for $x \in [0, L]$ as

$$D\partial_x\left(\pi R^2(x)\partial_x\bar{\rho}_s(x) - 2\pi R(x)\sigma\frac{e\partial_x\bar{\psi}}{k_B T}\right) - Q\partial_x\bar{\rho}_s(x) = 0. \tag{3}$$

Here, we use the radial independence of $\rho_s(x,r)$ and $\psi(x,r)$ in the thin-EDL limit as well as the slab-neutrality condition $2\pi\int_0^{R(x)}\rho_e(x,r)r\mathrm{d}r = -2\pi R(x)\sigma$ as derived in part (II) of the supplementary material. The slab neutrality condition is an important difference with the analysis presented in Ref. 46, where it was suggested that a bulk space-charge is of key importance for understanding the observed mechano-sensitivity of conical pores. For a given ΔP and $\Delta\psi$, we consider Q and $\partial_x\bar{\psi}(x)$ known from Eqs. (1) and (2), respectively, such that Eq. (3) is an ordinary second-order differential equation for $\bar{\rho}_s(x)$; together with its solutions presented below, it constitutes the key result of this Letter. An important role will be played by the conductive contribution $J_{cond}(x)$ to J given by $J_{cond}(x) = -2\pi D\sigma(e\Delta\psi/k_B T)R_b R_t/R(x)L$, which varies with x in a conical channel and, thus, acts as a source or sink term in Eq. (3) that sucks ions into the channel for $\Delta\psi < 0$ and pushes them out for $\Delta\psi > 0$.

Given the long-channel limit of interest and the equal salinity of both reservoirs, we solve Eq. (3) with boundary conditions $\bar{\rho}_s(0) = \bar{\rho}_s(L) = 2\rho_b$, resulting in

$$\begin{aligned}\bar{\rho}_s(x) - 2\rho_b &= \frac{\Delta\rho}{\mathrm{Pe}}\left[\frac{x}{L}\frac{R_t}{R(x)} - \frac{\exp\left(\frac{x}{L}\frac{R_t^2}{R_b R(x)}\mathrm{Pe}\right) - 1}{\exp\left(\frac{R_t}{R_b}\mathrm{Pe}\right) - 1}\right] \\ &= \begin{cases} \frac{\Delta\rho}{2}\frac{x}{L}\left(1 - \frac{x}{L}\right)\frac{R_t^2}{R^2(x)} & \text{if } |\mathrm{Pe}| \ll \left(\frac{R_b}{R_t}\right)^2, \\ \frac{\Delta\rho}{2|\mathrm{Pe}|}\left(\frac{R_b}{R(x)}\left(1 - \frac{x}{L}\left(1 + \frac{R_t}{R_b}\right)\right) \mp 1\right) & \text{if } \pm\mathrm{Pe} \gg \left(\frac{R_b}{R_t}\right)^2. \end{cases}\end{aligned} \tag{4}$$

Here, we not only introduced the tip Péclet number $\mathrm{Pe} \equiv QL/D\pi R_t^2$ with $Q(\Delta P, \Delta\psi)$ given by Eq. (1) but also a measure for the concentration inhomogeneity

$$\Delta\rho \equiv \frac{2(R_b - R_t)\sigma}{R_t^2}\frac{e\Delta\psi}{k_B T}, \tag{5}$$

thus, $\Delta\rho = 0$ if $R_b = R_t$ and hence $\bar{\rho}_s(x) = 2\rho_b$ in this case. Note that both Pe and $\Delta\rho$ have a sign and that the dependence on the potential drop is not only accounted for by $\Delta\rho$ but also by Pe through the electro-osmotic contribution to Q [see Eq. (1)]. Clearly, Eq. (4) reveals concentration variations on length scales on the order of the full channel length $0 \le x \le L$, most prominently for smaller $|\mathrm{Pe}|$. Since the Péclet number quantifies the importance of flow, we can now reconcile the discrepancy between works which find electro-osmotic flow to be negligible[48] and others which find it to be important,[53] as the former concerns a parameter set with small $\mathrm{Pe} \simeq 10^{-2}(R_b/R_t)^2$ and the latter with large $\mathrm{Pe} \simeq 3(R_b/R_t)^2$. For $\Delta\psi = \pm 0.4$ V, which for our standard parameter set gives $\Delta\rho = \mp 31$ mM from Eq. (5), we plot the concentration profile $\bar{\rho}_s(x)$ of Eq. (4) in Fig. 2(a) for Péclet numbers between 0 and ∓ 200. In Fig. 2(b), we plot the salt concentration $\langle\bar{\rho}_s\rangle$ laterally averaged over the interval $x \in [0, L]$, which will play a key role in the electric conductivity $\mathbb{L}_{22}$, as a function of the imposed pressure drop ΔP for the three voltage drops $\Delta\psi = +0.4$ V (red), 0 V (green), and -0.4 V (blue), as obtained numerically from solutions of the PNPS equations (symbols) and on the basis of a straightforward numerical integration of Eq. (4) (lines). The agreement, although not perfect, is very good especially for $\Delta P > 0$. Our Eq. (4) not only correctly predicts the increase/decrease compared to $2\rho_b$ for a negative/positive potential drop but also the non-monotonic dependence on ΔP; the absolute difference with $2\rho_b$ is largest (and on the order of 30%) for $\Delta P \simeq \mp 10$ mbar, which corresponds in both cases to $\mathrm{Pe} \simeq 0$. The two vertical dashed lines represent the pressure drop $\Delta P^* = -(\mathbb{L}_{12}/\mathbb{L}_{11})\Delta\psi$, where $Q = 0$ and hence $\mathrm{Pe} = 0$ on the basis of Eq. (1), such that the optimal concentration polarization is to be expected. Collecting our earlier results, we find the optimal pressure drop per voltage drop

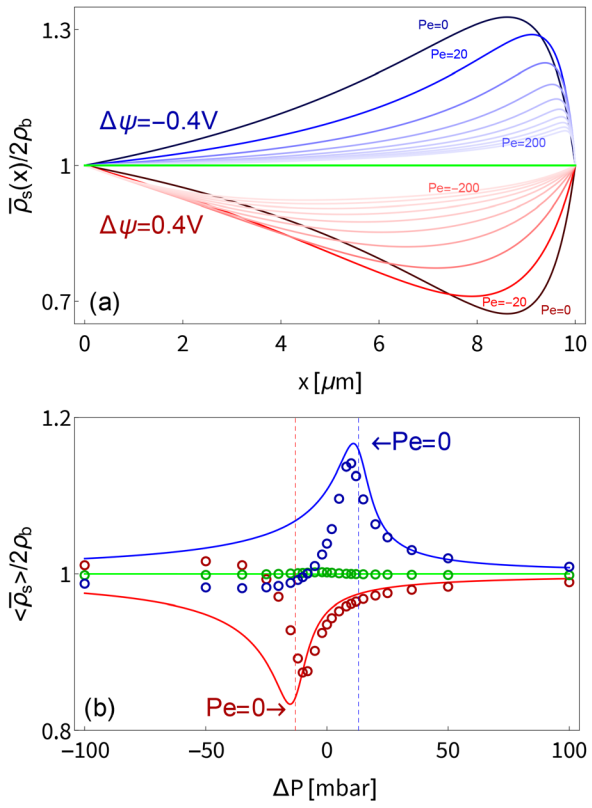

FIG. 2. (a) Cross-sectional averaged salt concentration $\bar{\rho}_s(x)$ normalized by the bulk concentration $2\rho_b$ as a function of the lateral position x for our standard parameter set (see the text). For potential drops, $\Delta\psi = +0.4$ V (red) and -0.4 V (blue), for which $\Delta\rho = \mp 31$ mM according to Eq. (5), the solid lines represent concentration profiles at Péclet numbers that vary between 0 and ∓ 200 in steps of 20. The green curve represents the case $\Delta\psi = 0$ V at any Pe. (b) The normalized laterally averaged concentration $\langle\bar{\rho}_s\rangle/2\rho_b$ as a function of the pressure drop ΔP at potential drops $\Delta\psi = +0.4$ V (red), –0.4 V (blue), and 0 V (green). The solid lines represent Eq. (4), data points are from numerical solutions to the full PNPS equations, which for $\Delta\psi = \pm 0.4$ V show an extremum very close to $\Delta P^* = \mp 13$ mbar from Eq. (6) where Pe = 0, denoted by the vertical dashed lines.

$$\frac{\Delta P^*}{\Delta\psi} = \varepsilon\psi_0 \frac{8(R_b^2 + R_b R_t + R_t^2)}{3R_b^2 R_t^2} \overset{R_b \gg R_t}{\simeq} \frac{8\varepsilon\psi_0}{3R_t^2}, \tag{6}$$

which yields about -32mbar/V for our standard parameter set and about -27 mbar/V for the extremely large tip-base ratios $R_b \gg R_t$ generated by the extrusion of a pipette in the experiments of Ref. 46 (if we assume $\psi_0 = -40$ mV common for silica[63]). Clearly, the inverse square scaling of ΔP^* with R_t is key to explaining the dramatic pressure-sensitivity observed in the experiments.[46] In fact, our results suggest even more pressure-sensitivity for larger conical channels, e.g., for $R_t = 10\mu$m, we have ΔP^* in the microbar regime, which can already be exerted by the sound of passing traffic.[68,69] For cases where $\Delta P \gg \Delta P^*$, concentration polarization is washed out by the flow; variation of current with both pressure and voltage then closely follows Ohmic conduction. As flow suppresses diodic performance, at a static pressure drop, $\Delta P \neq \Delta P^*$ rectification can also be increased by lowering the dielectric constant ε or increasing the viscosity η thereby lowering the electro-osmotic flow rate while keeping $\Delta\rho$ unchanged.

Now that we have established that Eq. (4) gives a fair account of the salt concentration profile in the channel, we will use it to approximate $\mathbb{L}_{22}$. In the thin-EDL limit, the total current I is dominated by the conductive component $-(De/k_BT)\rho_s(x,r)\partial_x\psi(x,r)$ of $\hat{\mathbf{x}}\cdot e\mathbf{j}_e(x,r)$ and cross-sectional integration of this current with Eq. (2) and the same thin-EDL limit as before yields $I_{cond}(x) = \pi R_b R_t eD\bar{\rho}_s(x)(e\Delta\psi/k_BTL)$, which manifestly depends on x on the basis of Eq. (4). In steady state, this lateral variation of the conductive

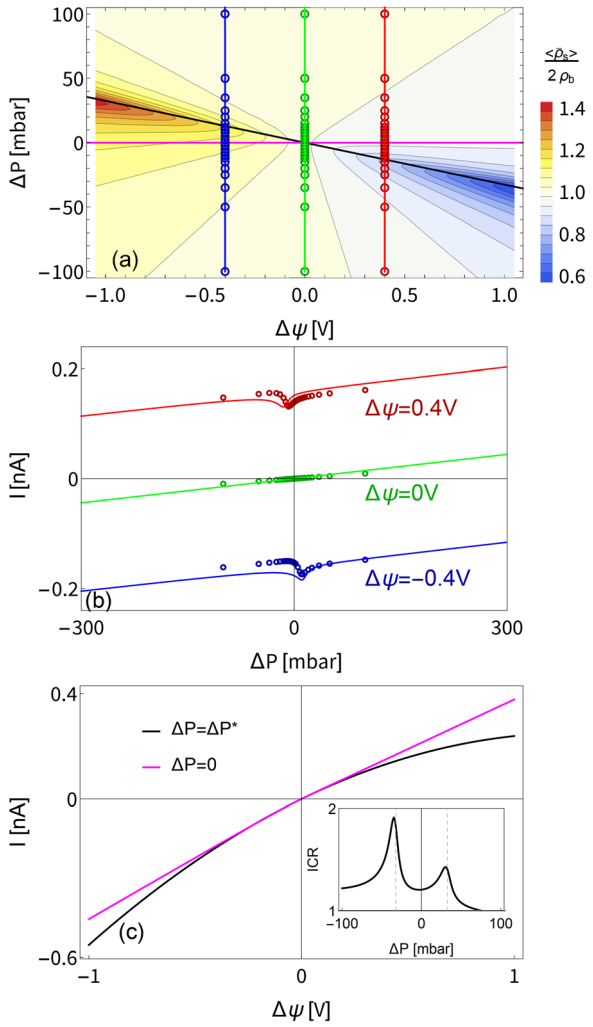

FIG. 3. (a) Heat map of the laterally averaged salt concentration $\langle\overline{\rho_s}\rangle$ for the standard parameter set (see the text) in the potential drop $\Delta\psi$—pressure drop ΔP plane. (b) Current–pressure ($I - \Delta P$) relation for three fixed potential drops showing a minimum close to $\Delta P = \Delta P^*$ of Eq. (6). The symbols represent numerical solutions to the full PNPS equations at parameter combinations shown in (a) and the solid lines represent our analytic solution based on Eq. (1). (c) Current–voltage ($I - \Delta\psi$) relation for $\Delta P = 0$ (pink) and the optimal pressure drop $\Delta P = \Delta P^*$ (black) which shows increased current rectification ICR compared to $\Delta P = 0$. The inset shows the pressure drop dependence of the ICR$= -I(-1\text{ V})/I(1\text{ V})$, which exhibits two maxima at $\Delta P = \pm\Delta P^*$.

current must be compensated by diffusive and advective currents and the resulting laterally invariant current I can be obtained by treating the concentration profile $\bar{\rho}_s(x)$ as a collection of resistors in series,[67] such that $\mathbb{L}_{22} = (De^2/k_BT)\langle\bar{\rho}_s\rangle$, which reveals that conductance is proportional to the laterally averaged salt concentration.

For our standard parameter set, we plot $\langle\bar{\rho}_s\rangle$ in Fig. 3(a) as a heat map in the $(\Delta\psi, \Delta P)$ plane, including a few iso-concentration contours. We clearly see the largest concentration variations, and hence the largest variations of $\mathbb{L}_{22}$, along the black line that represents $\Delta P = \Delta P^*$ of Eq. (6). In Fig. 3(b), we plot the ΔP-dependence of the electric current I (lines) as predicted from Eq. (1) for three voltage drops (± 0.4 V and zero), together with full numerical calculations (symbols) at the state points indicated by the color-matching symbols in Figs. 3(a), 3(b), and 2(b). The overall agreement is quantitative at $\Delta\psi = 0$, which is fully in the linear-response regime, while the nonlinear gross features at $\Delta\psi = \pm 0.4$ V, especially at $\Delta P \simeq \Delta P^* \simeq \mp 13$ mbar, are accounted for with reasonable accuracy, the more so at the positive potential drop. In Fig. 3(c), we plot current–voltage relations at pressure drops $\Delta P = 0$ and $\Delta P = \Delta P^*$, using the same color coding as in Fig. 3(a). The degree of non-Ohmic behavior, characterized by the ionic current rectification ICR $= -I(-1V)/I(1V)$, is clearly larger at the optimal pressure drop ΔP^*, which is indeed borne out by the inset which shows the full ΔP dependence of ICR, revealing peaks at $\pm\Delta P^*$.

Finally, using our explicit knowledge of $\langle\bar{\rho}_s\rangle$ and the full transport matrix of Eq. (1), we can explicitly search for an optimal cone geometry at which the deviation from Ohmic conductance is largest. Naively, Eq. (5) suggests that for a large concentration profile the ideal tip-to-base ratio should be small ($R_t/R_b \ll 1$); however, Eq. (4) shows that in this limit the concentration profile becomes localized near the tip resulting in a small channel-averaged concentration change. The ideal pore geometry balances the magnitude and spread of the concentration profile and in part (III) of the supplementary material, we show that this optimum occurs at a universal tip-to-base ratio $R_t/R_b \simeq 0.22$ for $|\mathrm{Pe}| \lesssim 1$. The optimum ratio for concentration polarization decreases as the power law $b|\mathrm{Pe}|^{-\nu}$ with $b = 2.5$ and $\nu = 0.9$ for $\mathrm{Pe} \geq 10^2$ and $b = 0.9$ and $\nu = 0.55$ for $\mathrm{Pe} \leq -10^2$; for all flow rates, the ideal tip-to-base ratio is less than 0.22. Interestingly, the ideal pore geometry is independent of the channel length L, which follows from our Eq. (4) for $\bar{\rho}_s(x)$ that only depends on x/L, such that $\mathbb{L}_{22}$ (and in fact the whole matrix $\mathbb{L}$) is independent of the channel length. Hence the concentration polarization does not depend on the cone opening angle, which is surprising as most authors identify it as the key geometric parameter controlling pressure-sensitivity[46] and current rectification.[49,70]

In conclusion, we provide a full microscopic understanding of the ultra-sensitive pressure and voltage dependence of the electric conductivity of cone-shaped channels. We identify and quantify concentration polarization due to geometric frustration which leads to a source term in Eq. (3), even in the thin-EDL case considered here. Moreover, we found an optimal channel geometry $R_t/R_b \simeq 0.22$ and an optimal operation condition Eq. (6) for current rectification. These insights are important for further developments of mechano-tronic[43,44,71] and biochemical[31–33] sensing as well as microfluidic[7,8] and neuromorphic applications.[39,72]

SUPPLEMENTARY MATERIAL

See the supplementary material for (I) the full Poisson–Nernst–Planck–Stokes equations, (II) a detailed derivation of the Onsager matrix $\mathbb{L}$, (III) a detailed derivation of the optimal pore geometry, and (IV) a discussion of our full numerical results.

ACKNOWLEDGMENTS

This work was a part of the D-ITP consortium, a program of the Netherlands Organisation for Scientific Research (NWO) that is funded by the Dutch Ministry of Education, Culture and Science (OCW).

AUTHOR DECLARATIONS

Conflict of Interest

The authors have no conflicts to disclose.

Author Contributions

Willem Boon and Tim Veenstra contributed equally to this paper.

Willem Q. Boon: Conceptualization (equal); Formal analysis (equal); Investigation (equal); Visualization (lead); Writing – original draft (lead); Writing – review & editing (lead). **Tim E. Veenstra:** Data curation (lead); Formal analysis (equal); Investigation (equal); Visualization (supporting); Writing – original draft (supporting). **Marjolein Dijkstra:** Funding acquisition (lead); Project administration (lead); Supervision (lead); Writing – review & editing (equal). **René van Roij:** Funding acquisition (lead); Project administration (lead); Supervision (lead); Writing – review & editing (equal).

DATA AVAILABILITY

The data that support the findings of this study are available within the article and its supplementary material.

REFERENCES

[1] Z. Zhang, L. Wen, and L. Jiang, "Nanofluidics for osmotic energy conversion," Nat. Rev. Mater. **6**, 622 (2021).
[2] D.-K. Kim, C. Duan, Y.-F. Chen, and A. Majumdar, "Power generation from concentration gradient by reverse electrodialysis in ion-selective nanochannels," Microfluid. Nanofluid. **9**, 1215 (2010).
[3] A. Siria, P. Poncharal, A.-L. Biance, R. Fulcrand, X. Blase, S. T. Purcell, and L. Bocquet, "Giant osmotic energy conversion measured in a single transmembrane boron nitride nanotube," Nature **494**, 455 (2013).
[4] A. Siria, M.-L. Bocquet, and L. Bocquet, "New avenues for the large-scale harvesting of blue energy," Nat. Rev. Chem. **1**, 0091 (2017).
[5] M. Elimelech and W. A. Phillip, "The future of seawater desalination: Energy, technology, and the environment," Science **333**, 712 (2011).
[6] A. Campione, L. Gurreri, M. Ciofalo, G. Micale, A. Tamburini, and A. Cipollina, "Electrodialysis for water desalination: A critical assessment of recent developments on process fundamentals, models and applications," Desalination **434**, 121 (2018).
[7] X. Wang, C. Cheng, S. Wang, and S. Liu, "Electroosmotic pumps and their applications in microfluidic systems," Microfluid. Nanofluid. **6**, 145 (2009).
[8] T. M. Squires and S. R. Quake, "Microfluidics: Fluid physics at the nanoliter scale," Rev. Mod. Phys. **77**, 977 (2005).
[9] L. Bocquet and E. Charlaix, "Nanofluidics, from bulk to interfaces," Chem. Soc. Rev. **39**, 1073 (2010).
[10] R. B. Schoch, J. Han, and P. Renaud, "Transport phenomena in nanofluidics," Rev. Mod. Phys. **80**, 839 (2008).
[11] J. C. Eijkel and A. van den Berg, "Nanofluidics: What is it and what can we expect from it?," Microfluid. Nanofluid. **1**, 249 (2005).

[12]B. L. Werkhoven, J. C. Everts, S. Samin, and R. van Roij, "Flow-induced surface charge heterogeneity in electrokinetics due to stern-layer conductance coupled to reaction kinetics," Phys. Rev. Lett. **120**, 264502 (2018).
[13]B. L. Werkhoven, S. Samin, and R. van Roij, "Dynamic Stern layers in charge-regulating electrokinetic systems: Three regimes from an analytical approach," Eur. Phys. J. Spec. Top. **227**, 2539 (2019).
[14]P. Ober, W. Q. Boon, M. Dijkstra, E. H. Backus, R. van Roij, and M. Bonn, "Liquid flow reversibly creates a macroscopic surface charge gradient," Nat. Commun. **12**(1), 4102 (2021).
[15]S. Levine, J. Marriott, G. Neale, and N. Epstein, "Theory of electrokinetic flow in fine cylindrical capillaries at high zeta-potentials," J. Colloid Interface Sci. **52**, 136 (1975).
[16]M. Sadeghi, M. H. Saidi, and A. Sadeghi, "Electroosmotic flow and ionic conductance in a pH-regulated rectangular nanochannel," Phys. Fluids **29**, 062002 (2017).
[17]M. Sadeghi, M. H. Saidi, A. Moosavi, and A. Sadeghi, "Geometry effect on electrokinetic flow and ionic conductance in pH-regulated nanochannels," Phys. Fluids **29**, 122006 (2017).
[18]S. Chanda and P. A. Tsai, "Competition between electroosmotic and chemiosmotic flow in charged nanofluidics," Phys. Fluids **33**(3), 032008 (2021).
[19]N. Laohakunakorn, V. V. Thacker, M. Muthukumar, and U. F. Keyser, "Electroosmotic flow reversal outside glass nanopores," Nano Lett. **15**, 695 (2015).
[20]W.-J. Lan, M. A. Edwards, L. Luo, R. T. Perera, X. Wu, C. R. Martin, and H. S. White, "Voltage-rectified current and fluid flow in conical nanopores," Acc. Chem. Res. **49**, 2605 (2016).
[21]G. W. Bishop, M. M. Lopez, Jr., P. Ramiah Rajasekaran, X. Wu, and C. R. Martin, "Electroosmotic flow rectification in membranes with asymmetrically shaped pores: Effects of current and pore density," J. Phys. Chem. C **119**, 16633 (2015).
[22]Z. Asghar, M. Waqas, M. A. Gondal, and W. A. Khan, "Electro-osmotically driven generalized Newtonian blood flow in a divergent micro-channel," Alexandria Eng. J. **61**, 4519 (2022).
[23]Z. Asghar, M. W. Saeed Khan, M. A. Gondal, and A. Ghaffari, "Channel flow of non-Newtonian fluid due to peristalsis under external electric and magnetic field," Proc. Inst. Mech. Eng., Part E (published online 2022).
[24]H. S. White and A. Bund, "Ion current rectification at nanopores in glass membranes," Langmuir **24**, 2212 (2008).
[25]C. Wen, S. Zeng, S. Li, Z. Zhang, and S.-L. Zhang, "On rectification of ionic current in nanopores," Anal. Chem. **91**, 14597 (2019).
[26]J. E. Proctor, "Theory of ion transport and ion current rectification in nanofluidic diodes," MSc thesis (Clemson University, 2021).
[27]D. Woermann, "Electrochemical transport properties of a cone-shaped nanopore: High and low electrical conductivity states depending on the sign of an applied electrical potential difference," Phys. Chem. Chem. Phys. **5**, 1853 (2003).
[28]D. Woermann, "Electrochemical transport properties of a cone-shaped nanopore: Revisited," Phys. Chem. Chem. Phys. **6**, 3130 (2004).
[29]M. L. Kovarik, K. Zhou, and S. C. Jacobson, "Effect of conical nanopore diameter on ion current rectification," J. Phys. Chem. B **113**, 15960 (2009).
[30]C.-Y. Lin, L.-H. Yeh, and Z. S. Siwy, "Voltage-induced modulation of ionic concentrations and ion current rectification in mesopores with highly charged pore walls," J. Phys. Chem. Lett. **9**, 393 (2018).
[31]I. Vlassiouk, T. R. Kozel, and Z. S. Siwy, "Biosensing with nanofluidic diodes," J. Am. Chem. Soc. **131**, 8211 (2009).
[32]S. N. Bush, T. T. Volta, and C. R. Martin, "Chemical sensing and chemoresponsive pumping with conical-pore polymeric membranes," Nanomaterials **10**, 571 (2020).
[33]X. Hou, W. Guo, and L. Jiang, "Biomimetic smart nanopores and nanochannels," Chem. Soc. Rev. **40**, 2385 (2011).
[34]A. Piruska, M. Gong, J. V. Sweedler, and P. W. Bohn, "Nanofluidics in chemical analysis," Chem. Soc. Rev. **39**, 1060 (2010).
[35]M. Gholinejad, A. J. Moghadam, and S. A. Mousavi Shaegh, "Analysis of preconcentration patterns in microfluidic ion concentration polarization devices," Phys. Fluids **34**, 012014 (2022).
[36]M. Gholinejad, A. Jabari Moghadam, D.-T. Phan, A. K. Miri, and S. A. Mousavi Shaegh, "Design and application of ion concentration polarization for preconcentrating charged analytes," Phys. Fluids **33**, 051301 (2021).
[37]M. Gholinejad, A. Jabari Moghadam, S. A. Mousavi Shaegh, and A. K. Miri, "Multifactorial analysis of ion concentration polarization for microfluidic preconcentrating applications using response surface method," Phys. Fluids **32**, 072012 (2020).
[38]Y. Gong, C. Zhang, X. Weng, B. Peng, and H. Jiang, "Electrokinetically induced concentration of diluted sample by liquid metal embedded microfluidic chip," Phys. Fluids **34**, 022006 (2022).
[39]C. Li, T. Xiong, P. Yu, J. Fei, and L. Mao, "Synaptic iontronic devices for brain-mimicking functions: Fundamentals and applications," ACS Appl. Bio Mater. **4**, 71 (2021).
[40]S. Ghosal, J. D. Sherwood, and H.-C. Chang, "Solid-state nanopore hydrodynamics and transport," Biomicrofluidics **13**, 011301 (2019).
[41]H. Chun and T. D. Chung, "Iontronics," Annu. Rev. Anal. Chem. **8**, 441 (2015).
[42]J. Jung, J. Kim, J. Lee, Y.-W. Oh, S. Jung, I.-S. Kang, and K. Choi, "Modulation of ionic current rectification direction for biomimetic aluminum oxide membrane by surface modification," AIP Adv. **12**, 035141 (2022).
[43]C. D. Cox, N. Bavi, and B. Martinac, "Biophysical principles of ion-channel-mediated mechanosensory transduction," Cell Rep. **29**(1), 1 (2019).
[44]A. Anishkin, S. H. Loukin, J. Teng, and C. Kung, "Feeling the hidden mechanical forces in lipid bilayer is an original sense," Proc. Natl. Acad. Sci. U. S. A. **111**, 7898 (2014).
[45]F. Qian, W. Zhang, D. Huang, W. Li, Q. Wang, and C. Zhao, "Electrokinetic power generation in conical nanochannels: Regulation effects due to conicity," Phys. Chem. Chem. Phys. **22**, 2386 (2020).
[46]L. Jubin, A. Poggioli, A. Siria, and L. Bocquet, "Dramatic pressure-sensitive ion conduction in conical nanopores," Proc. Natl. Acad. Sci. U. S. A. **115**, 4063 (2018).
[47]D. Pandey and S. Bhattacharyya, "Influence of finite ion size and dielectric decrement on the ion current rectification in a single conical nanopore," Phys. Fluids **33**, 062006 (2021).
[48]W.-J. Lan, D. A. Holden, and H. S. White, "Pressure-dependent ion current rectification in conical-shaped glass nanopores," J. Am. Chem. Soc. **133**, 13300 (2011).
[49]C. Kubeil and A. Bund, "The role of nanopore geometry for the rectification of ionic currents," J. Phys. Chem. C **115**, 7866 (2011).
[50]I. Vlassiouk, S. Smirnov, and Z. Siwy, "Nanofluidic ionic diodes. Comparison of analytical and numerical solutions," ACS Nano **2**, 1589 (2008).
[51]P. Ramirez, P. Y. Apel, J. Cervera, and S. Mafé, "Pore structure and function of synthetic nanopores with fixed charges: Tip shape and rectification properties," Nanotechnology **19**, 315707 (2008).
[52]J. Cervera, B. Schiedt, R. Neumann, S. Mafé, and P. Ramírez, "Ionic conduction, rectification, and selectivity in single conical nanopores," J. Chem. Phys. **124**, 104706 (2006).
[53]D.-H. Lin, C.-Y. Lin, S. Tseng, and J.-P. Hsu, "Influence of electroosmotic flow on the ionic current rectification in a pH-regulated, conical nanopore," Nanoscale **7**, 14023 (2015).
[54]J.-P. Hsu, S.-T. Yang, C.-Y. Lin, and S. Tseng, "Ionic current rectification in a conical nanopore: Influences of electroosmotic flow and type of salt," J. Phys. Chem. C **121**, 4576 (2017).
[55]Y. Ai, M. Zhang, S. W. Joo, M. A. Cheney, and S. Qian, "Effects of electroosmotic flow on ionic current rectification in conical nanopores," J. Phys. Chem. C **114**, 3883 (2010).
[56]W. Brown, M. Kvetny, R. Yang, and G. Wang, "Higher ion selectivity with lower energy usage promoted by electro-osmotic flow in the transport through conical nanopores," J. Phys. Chem. C **125**, 3269 (2021).
[57]M. Aarts, W. Boon, B. Cuénod, M. Dijkstra, R. van Roij, and E. Alarcon-Llado, arXiv:2206.14594 (2022).
[58]E. Choi, C. Wang, G. T. Chang, and J. Park, "High current ionic diode using homogeneously charged asymmetric nanochannel network membrane," Nano Lett. **16**, 2189 (2016).
[59]S. Dal Cengio and I. Pagonabarraga, "Confinement-controlled rectification in a geometric nanofluidic diode," J. Chem. Phys. **151**, 044707 (2019).
[60]A. R. Poggioli, A. Siria, and L. Bocquet, "Beyond the tradeoff: Dynamic selectivity in ionic transport and current rectification," J. Phys. Chem. B **123**, 1171 (2019).
[61]F. Xiang, W. Zhang, X. Yang, and S. Liang, "Ionic current rectification: A result of the series connection of nanochannels with different Dukhin numbers," J. Phys. Chem. B **126**, 1779 (2022).

[62]A. W. Adamson and A. P. Gast, *Physical Chemistry of Surfaces* (Interscience Publishers, New York, 1967), Vol. 150.
[63]R. K. Iler, *The Colloid Chemistry of Silica and Silicates* (Cornell University Press, 1955), Vol. 80.
[64]M.-S. Chun, S.-Y. Lee, and S.-M. Yang, "Estimation of zeta potential by electrokinetic analysis of ionic fluid flows through a divergent microchannel," J. Colloid Interface Sci. **266**, 120 (2003).
[65]J. Happel and H. Brenner, *Low Reynolds Number Hydrodynamics: With Special Applications to Particulate Media* (Springer Science & Business Media, 2012), Vol. 1.
[66]T. E Veenstra, "Strongly non-linear pressure-induced ion currents in conical nanopores," BSc thesis (Utrecht University, 2020).
[67]B. L. Werkhoven and R. van Roij, "Coupled water, charge and salt transport in heterogeneous nano-fluidic systems," Soft Matter **16**, 1527 (2020).
[68]M. W. Khan, M. A. Memon, M. N. Khan, and M. M. Khan, "Traffic noise pollution in Karachi, Pakistan," J. Liaquat Univ. Med. Health Sci. **9**, 114 (2010).
[69]D. A. Bies, C. H. Hansen, and C. Q. Howard, *Engineering Noise Control* (CRC Press, 2017).
[70]J. M. Perry, K. Zhou, Z. D. Harms, and S. C. Jacobson, "Ion transport in nanofluidic funnels," ACS Nano **4**, 3897 (2010).
[71]A. Marcotte, T. Mouterde, A. Niguès, A. Siria, and L. Bocquet, "Mechanically activated ionic transport across single-digit carbon nanotubes," Nat. Mater. **19**, 1057 (2020).
[72]P. Robin, N. Kavokine, and L. Bocquet, "Modeling of emergent memory and voltage spiking in ionic transport through angstrom-scale slits," Science **373**, 687 (2021).